

Dinuclear Copper Complex with a Pyridazine-Bridged Octadentate Ligand: Monooxygenase Activity and Characterization of Copper-Oxygen Intermediates

Alexander Stüber,^[a] Ramona Jurgeleit,^[a] Benjamin Grimm-Lebsanft,^[b] Sören Buchenau,^[b] Ina Kellner,^[c] Yannik Appiarius,^[d, e] Christian Näther,^[a] Jan Krahmer,^[a] Ivana Ivanović-Burmazović,^[c] Michael Rübhausen,^{*[b]} Maria A. Naumova,^{*[f]} and Felix Tuczek^{*[a]}

Copper-containing enzymes catalyze the mono-oxygenation of aromatic and aliphatic substrates in nature. Herein, we report on the synthesis of a new dinuclear copper complex supported by an octadentate ligand with a pyridazine backbone. Low-temperature oxygenation leads to a μ -1,1-hydroperoxo dicopper(II) (Cu_2OOH) complex, which in turn stoichiometrically converts anthrone (AT) to anthraquinone (AQ). Oxygenation at room temperature, by contrast, leads to a new species that mediates the conversion of AT to AQ in a catalytic fashion, but

neither corresponds to a μ -peroxo nor a mono μ -oxo dicopper complex. For further analysis, a μ -hydroxo dicopper(II) (Cu_2OH) complex is synthesized by oxidation of the copper(I) complex with AgOTf. The electronic and geometric structures of the Cu_2OOH and Cu_2OH intermediates, as well as the structure of the room-temperature oxygenation product are elucidated by UV/Vis, Raman, X-ray absorption spectroscopy (XAS), and mass spectrometry, coupled to DFT.

1. Introduction

The transformation of inert C—H bonds to useful products is one of the biggest challenges of chemistry.^[1] In this regard, copper-dependent monooxygenases play an important role, as exemplified by the enzyme particulate methane monooxygenase (pMMO) that converts methane to methanol in methanotrophic bacteria.^[2] However, the identity of the active site in pMMO is still subject to controversy, and details of the reaction mechanism have not fully been elucidated yet.^[2,3] On the other hand, mono- μ -oxo dicopper(II) (Cu_2O) species have been found to perform this challenging conversion in the inorganic solid-state system Cu-ZSM-5.^[4,5] This structural motif, therefore, is currently considered as one of the important copper-oxygen species besides the common Cu_2O_x cores.^[5–11] However, only a

few small-molecule Cu_2O model complexes have been established to date,^[6,11–13] and a comprehensive understanding of how the ligand sphere influences their electronic and reactive properties is lacking.^[6,7,11–15]

Recently we reported on dicopper(I) complexes supported by hexadentate ligands with a pyridazine backbone.^[11,13] Notably, these systems were found to exhibit catalytic monooxygenation activity, transferring both oxygen atoms of O_2 to aliphatic substrates without the need of additional reductant. Using a combination of UV/Vis, resonance-Raman (rR), and X-ray absorption spectroscopy (XAS) complemented by UHR-ESI mass spectrometry, we were able to show that dioxygen initially is bound as μ_4 -peroxide in a tetranuclear $\text{Cu(I)}_2\text{Cu(II)}_2$ cluster. Subsequent O—O bond cleavage leads to two mono- μ -oxo dicopper(II) complexes, which in turn oxygenate a variety of hydrocarbons with

[a] A. Stüber, Dr. R. Jurgeleit, Prof. Dr. C. Näther, J. Krahmer, Prof. Dr. F. Tuczek
Institute of Inorganic Chemistry, Christian-Albrechts-University of Kiel,
Max-Eyth-Straße 2 24118, Kiel, Germany
E-mail: ftuczek@ac.uni-kiel.de

[b] Dr. B. Grimm-Lebsanft, Dr. S. Buchenau, Prof. Dr. M. Rübhausen
Institut für Nanostruktur- und Festkörperphysik, Center for Free Electron
Laser Science (CFEL), Universität Hamburg, Luruper Chaussee 149 22761,
Hamburg, Germany
E-mail: mruebhausen@physnet.uni-hamburg.de

[c] Dr. I. Kellner, Prof. Dr. I. Ivanović-Burmazović
Department Chemie, Ludwig-Maximilians-Universität München,
Butenandtstrasse 5–13, Haus D 81377, München, Germany

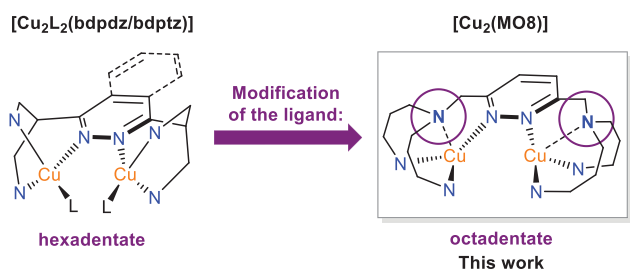
[d] Dr. Y. Appiarius
Institute for Organic and Analytical Chemistry, University of Bremen,
Leobener Strasse 7 28359, Bremen, Germany

[e] Dr. Y. Appiarius
MAPEX Center for Materials and Processes, University of Bremen,
Bibliothekstraße 1 28359, Bremen, Germany

[f] Dr. M. A. Naumova
DESY, Deutsches Elektronen-Synchrotron (DESY), Notkestrasse 85 22607,
Hamburg, Germany
E-mail: maria.naumova@desy.de

Supporting information for this article is available on the WWW under
<https://doi.org/10.1002/chem.202501659>

© 2025 The Author(s). Chemistry – A European Journal published by
Wiley-VCH GmbH. This is an open access article under the terms of the
Creative Commons Attribution License, which permits use, distribution and
reproduction in any medium, provided the original work is properly cited.

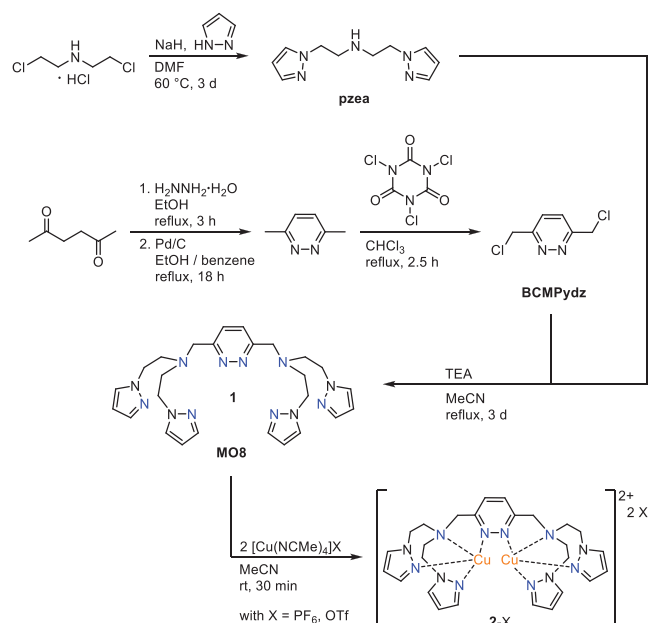


Scheme 1. Ligand design of MO8. The pyridine moieties of the (pyridazine-based) **bdpdz** and (phthalazine-based) **bdptz** systems (left) and the pyrazole rings of the **MO8** system (right) have been omitted for clarity and simplified by the *N*-donor atoms.

bond dissociation enthalpies (BDEs) below 82 kcal mol^{−1}.^[11] However, these **Cu₂O** intermediates exhibit a low thermal stability (up to −35°C), limiting the temperature range in which monooxygenation reactions can be conducted and, thus, their substrate scope.^[11] Hence, we wanted to modify the ligand sphere in order to make the **Cu₂O** species thermally more robust.

On this background, we synthesized a modified dinucleating ligand in which the two bidentate arms attached to the central pyridazine moiety of the original ligand are replaced by two tridentate NNN units, bound to the pyridazine via their central amines (cf Scheme 1). This modification of the parent system,^[11] which was based on the literature-known hexadentate ligands **bdpdz**^[16] and **bdptz**,^[17] leads to the octadentate ligand **MO8** (Scheme 1). In contrast to the terminal pyridine donors of the related octadentate, pyridazine-bridged ligand **BPMPD**,^[18] **MO8** is furnished with terminal pyrazole groups. We thought that the reduced σ -donor strength of pyrazole compared to pyridine may be beneficial for a more electrophilic and thus more reactive **Cu₂O** unit.^[19] Moreover, we expected that, due to its higher flexibility compared to **bdpdz/bdptz**, it might enable access to other copper-oxygen (**Cu₂O_x**) intermediates. Finally, we assumed that due to the two additional *N*-donor atoms, coordination of solvent ligands (as observed for the original system)^[11] might be reduced, thus enabling easier access of substrate to the **Cu₂O** moiety.

Having prepared **MO8**, we found that oxygenation of its dicopper(I) complex strongly depends on the temperature: upon reaction with O₂ at 183 K, a μ -1,1-hydroperoxo dicopper(II) complex (**Cu₂OOH**) is formed that decomposes at higher temperatures. By contrast, reaction with O₂ at room temperature leads to a new species that was first interpreted as a mono- μ -oxo dicopper(II) (**Cu₂O**) intermediate, based on its UV/Vis spectrum. Herein, the **Cu₂OOH** and **Cu₂OH** derivatives of the **Cu₂(MO8)** system as well as the room-temperature oxygenation product are structurally and/or spectroscopically characterized, and their monooxygenation activities toward various aliphatic substrates are examined. The results are compared with analogous data obtained on the original hexadentate **bdpdz/bdptz** system, and the electronic and structural factors determining the formation and stabilities of the copper-oxygen intermediates accessible in the **MO8** system as well as their respective reactivities are defined.



Scheme 2. Synthesis of the new octadentate *N*-donor ligand **MO8** 1 and formation of the corresponding dicopper(I) complexes **2-PF₆** and **2-OTf**.

2. Results and Discussion

2.1. Synthesis and Structural Characterization

2.1.1. Synthesis of the Ligand 1 and the Dicopper(I) Complex 2

The new multidentate *N*-donor ligand 3,6-bis(di(2-(1*H*-pyrazol-1-yl)ethyl)aminomethyl)pyridazine (**1**), denoted as **MO8**, was synthesized in a five-step procedure following the route shown in Scheme 2. The easily accessible *N,N*-bis((1*H*-pyrazol-1-yl)methyl)propane-1-amine (**pzea**)^[20] exhibits a central amine function, which is used to connect the two tridentate units to the 3,6-positions of a pyridazine spacer using 3,6-bis(chloromethyl)-pyridazine (**BCMPydz**)^[21] (Scheme 2).

Addition of two equivalents of [Cu(NCMe)₄]PF₆ or [Cu(NCMe)₄]OTf to the ligand in acetonitrile provided the complexes [Cu₂(**MO8**)](PF₆)₂ (**2-PF₆**) and [Cu₂(**MO8**)](OTf)₂ (**2-OTf**) in almost quantitative yields (Scheme 2 and Section S2.3).

2.1.2. Crystal Structure of 2-PF₆

Layering a solution of **2-PF₆** in acetone with diethyl ether yielded red crystals, which were investigated by single-crystal X-ray diffraction analysis.^[22] The obtained molecular structure reveals the expected tetracoordinated geometry for the copper(I) centers (see below, Figure 1, Section S3). Importantly, it does not show any additional solvent coligands, in contrast to the original **bdpdz/bdptz** system. This may also apply to the corresponding copper-oxygen intermediates (*vide infra*), potentially allowing easier substrate access to the active site than in the parent system.

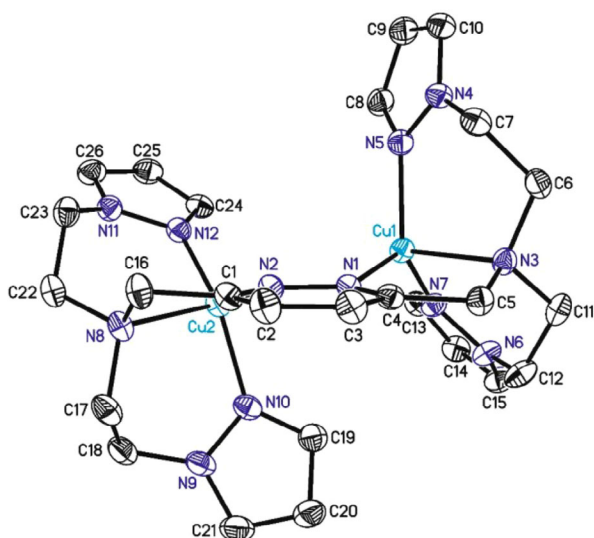


Figure 1. Crystal structure of the dicopper(I) complex $[\text{Cu}_2(\text{MO8})](\text{PF}_6)_2$ (2-PF_6). ORTEP plot of the cation in the crystal structure of compound 2-PF_6 with labeling and displacement ellipsoids drawn at the 50 % probability level. For clarity, the two crystallographically independent hexafluorophosphate anions and the hydrogen atoms are not shown.

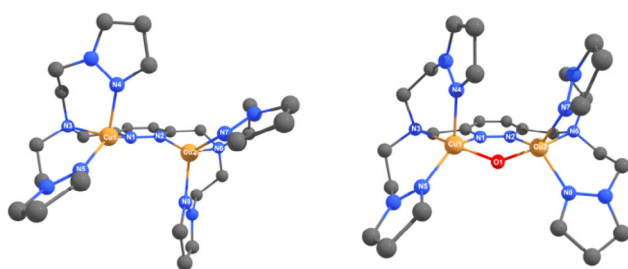


Figure 2. Geometry optimization of 2-PF_6 (left) and the corresponding Cu_2O species **4** (right). The hydrogen atoms have been omitted for clarity. DFT: RI-PBE-D3(BJ)/def2-SVP.^[23,24]

The coordination sphere of each copper center is distorted tetrahedral (Figure S21) and consists of four *N*-donor atoms, two of which derive from the pyrazole moieties and two from the amine and the pyridazine group, respectively (Figure 1). 2-PF_6 crystallizes in the monoclinic space group $\text{P}2_1/\text{n}$ with four units per unit cell. The average N-Cu-N angle is 106.38° , and the average Cu-N bond length is 2.0420 \AA , ranging from 1.9424 to 2.2229 \AA .^[22]

2.1.3. DFT Calculations

Geometry optimization of 2-PF_6 leads to a structure with Cu—Cu and Cu—N bond lengths comparable to the crystal structure of 2-PF_6 (see Figure 2, left, Table S14). Geometry optimization of the Cu_2O complex **4** of 2-PF_6 , on the other hand, indicates that a dicopper mono- μ -oxo core can be accommodated by the octadentate system of **MO8** (see Figure 2, right). Interestingly, the bond lengths of the Cu—N_{Amine} bond are about $0.2\text{--}0.3 \text{ \AA}$ longer than those of the other Cu—N bonds, suggesting a hemi-labile character of this bond (see Table S11).

2.1.4. Generation and Properties of the μ -Hydroxo Dicopper(II) Complex **3**

To gain further structural insight into our system, we prepared the μ -hydroxo dicopper(II) complexes $[\text{Cu}_2(\text{MO8})(\text{OH})]\text{X}_3$ (**3-X**, X = OTf or PF_6 ; Cu_2OH) by reaction of 2-OTf with AgOTf (or 2-PF_6 with AgPF_6 , respectively), in methanol, analogous to the procedure of Kuzelka et al.^[25] (cf Scheme 3). After the addition of 2 eq. of AgX to the respective Cu(I) complex **2-X**, the solution turned greenish within a few seconds.^[25] The resulting complexes were characterized by x-ray powder diffraction, UV/Vis-, NMR-, and IR-spectroscopy, as well as HR-ESI mass spectrometry and XAS. It should be noted that no additional source of oxygen was added so that the hydroxido ligand probably originates from traces of water being present in the solvent, as assumed by Kuzelka. The remaining proton then presumably forms HOTf (or HPF_6), which is eliminated upon drying in vacuo.

2.1.5. Crystal Structure of 3-PF_6

Turquoise-colored crystals were obtained by layering a solution of 3-PF_6 in acetone with *n*-hexane, which were investigated by single-crystal X-ray diffraction analysis. The crystal structure shows that each copper is pentacoordinated in 3-PF_6 and that the two copper centers are bridged via a hydroxido ligand (Figure 3, see below). As in the Cu(I)-complex 2-PF_6 , no additional solvent coligands coordinate to copper.

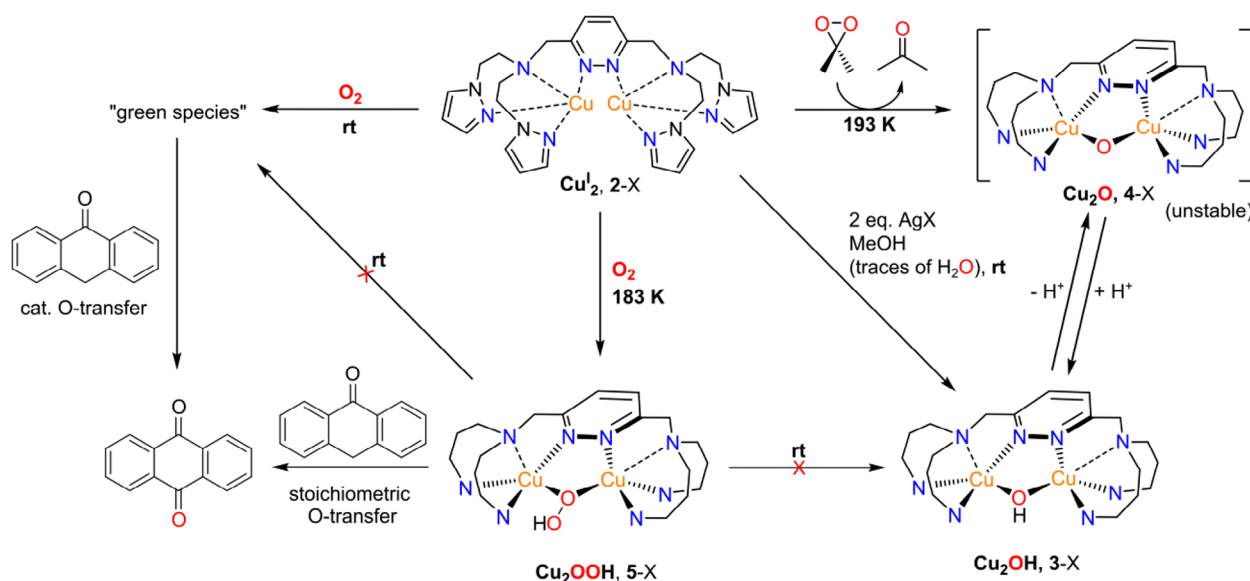
3-PF_6 crystallizes in the orthorhombic space group Pbcn with four units per unit cell. Both copper centers in 3-PF_6 exhibit a distorted square-pyramidal geometry (Figure S22). The average N-Cu-N angle is 104.70° and the average Cu-N bond length is 2.0522 \AA , ranging from 1.9843 to 2.1296 \AA . The Cu-O-Cu angle is 124.74° and the Cu-O bond length 1.9301 \AA .^[22] Bulk 3-PF_6 is crystalline, exhibiting a powder diffractogram that matches the corresponding crystal structure (Figure S23), whereas 3-OTf is found to be amorphous (Figure S24).

2.1.6. Spectroscopic Characterization of **3**

The solution of the Cu_2OH complex 3-OTf in acetone exhibits three absorption bands in the UV/Vis spectrum at 367 nm ($\epsilon = 5800 \text{ M}^{-1}\text{cm}^{-1}$), 680 nm ($\epsilon = 170 \text{ M}^{-1}\text{cm}^{-1}$), and 860 nm ($\epsilon = 120 \text{ M}^{-1}\text{cm}^{-1}$) (Figure 4a). The spectrum of 3-PF_6 is very similar to that of 3-OTf . However, this compound has a significantly lower solubility than 3-OTf (Figure S26).

Paramagnetic broadening of the signals in the ^1H -NMR spectrum of 3-OTf and 3-PF_6 (Figure S15,S17) indicates the presence of Cu(II). Compared to the Cu(I) complex **2**, some signals have shifted in the ^1H -NMR-spectrum of **3**. Apart from small shifts of some signals, the ^1H -NMR spectra of 3-OTf and 3-PF_6 are very similar. In the ^{13}C -NMR spectrum of **3** (Figure S16, S18), no signals are visible due to the paramagnetic broadening, which makes it difficult to assign the signals of the ^1H -NMR spectrum.

From the solution of 3-OTf in acetonitrile- d_3 used for NMR spectroscopy, an IR spectrum was recorded as well. To ensure that the sample was not affected by oxygen or humidity from the air, a sealed cell was used, which was prepared under an



Scheme 3. Formation of different copper-oxygen intermediates of the new MO8 model system and associated reactivities. The counterions X are hexafluorophosphate (PF₆) or triflate (OTf). The charges of all complexes shown have been omitted for clarity, and the pyrazole units in 3-X, 4-X, and 5-X have been simplified by the N-donor atoms.

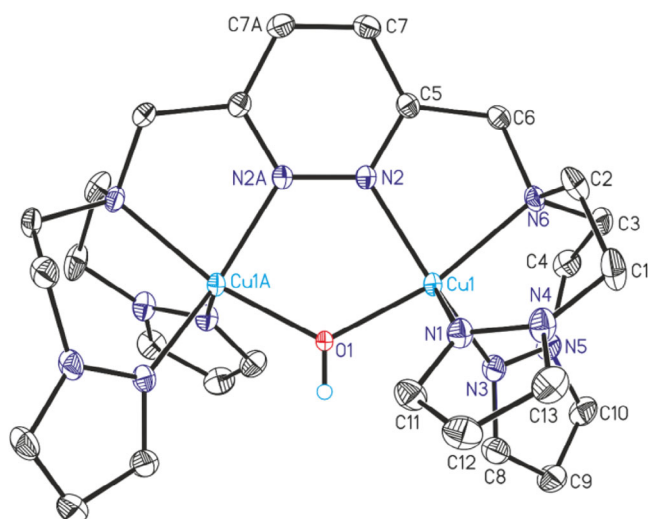


Figure 3. Crystal structure of the Cu₂OH complex [Cu₂(MO8)(OH)](PF₆)₃ (3-PF₆). ORTEP plot of the cation in the crystal structure of compound 3-PF₆ with labeling and displacement ellipsoids drawn at the 50 % probability level. For clarity the three crystallographically independent hexafluorophosphate anions and the hydrogen atoms (except from the OH group) are not shown.

inert atmosphere in the glovebox. The IR spectra of the 3-OTf and 2-OTf are very similar (Figure 4b/ Section S7.2). However, there is an additional absorption band at 3533 cm⁻¹ in the IR spectrum of 3-OTf (3530 cm⁻¹ for 3-PF₆) which lies in the range of an OH stretch.^[25–27] Bands corresponding to a symmetric (ν_s) or antisymmetric (ν_{as}) Cu–O stretch could not be identified clearly. DFT calculations indicate that ν_s should be around 423 cm⁻¹ and ν_{as} around 494 cm⁻¹. However, it was not possible to determine the Cu–O stretches using Raman or rRaman spectroscopy on solid samples due to the strong fluorescence.

2.1.7. HR-ESI-MS and XAS of 3

Since the Cu₂OH complex 3 is stable at room temperature, it was further investigated with HR-ESI mass spectrometry. In the mass spectrum of 3-OTf, a peak can be detected (calc. *m/z* 219.0544, obs. *m/z* 219.0540), the isotopic pattern and *m/z* value of which are consistent with the [Cu₂(MO8)(OH)]³⁺ species [3]³⁺ (Figure 4c). This trication is observed in the mass spectrum of 3-PF₆ as well (Figure S63). In addition, the bare [Cu₂(MO8)]²⁺ complex [2]²⁺ (calc. *m/z* 320.0805, obs. *m/z* 320.0801) and a peak that can be assigned to a [3-H₂O]³⁺ complex (calc. *m/z* 213.0509, obs. *m/z* 213.0506) (Figure S58,S59) are detected. These findings indicate that the Cu₂OH complex 3 might be protonated and eliminate the hydroxo ligand as H₂O in the mass spectrometer. Notably, a mono μ -oxo [Cu₂(MO8)O]²⁺ species [4]²⁺ (calc. *m/z* 328.0780, obs. *m/z* 328.0774) (Figure S60) is detected, too, which derives from deprotonation of the hydroxo complex 3 in the gas phase.

In order to differentiate a possible Cu₂O intermediate 4 present in homogeneous solution (cf Section 3) from the Cu₂OH complex 3, X-ray absorption near-edge structure spectroscopy (XANES) and extended X-ray absorption fine structure (EXAFS) analysis were employed. The XANES spectra of precursors 2-PF₆ and 2-OTf are typical for Cu(I) complexes (Figure 4d, 6d, 7b, 8b)^[28] and very similar to the **bdpdz/bdptz** system.^[11] For 2-OTf, the edge position measured at 50% of the edge jump (*E*_{1/2}) is at 8983.4 eV. A pronounced shoulder at ~8981.5 eV and a weaker shoulder at ~8985 eV are assigned to the electric-dipole allowed transitions from Cu 1s to Cu 4p orbitals.^[28–30,31] The EXAFS and XANES of 3-OTf are compatible with the presence of Cu(II) centers (Figure 4d). The edge position is shifted to a higher energy compared to 2-OTf (*E*_{1/2} = 8987.7 eV), and there is a pre-edge peak at 8977.9 eV. The emergence of a pre-edge is characteristic for both Cu(II) and Cu(III). However, Cu(III) compounds have

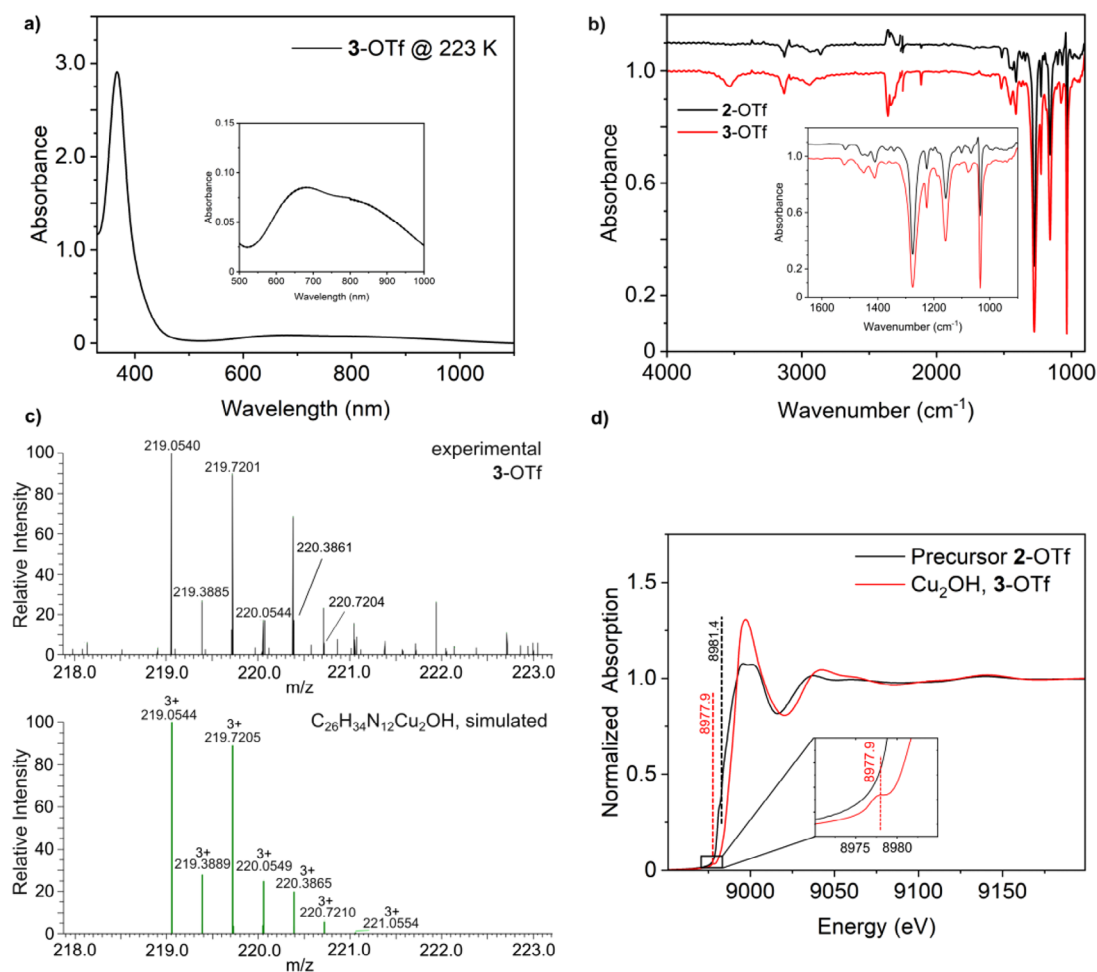


Figure 4. Characterization of the μ -hydroxo dicopper(II) complex **3**. a) Absorption spectra of an acetone solution of **3-OTf** at 223 K. b) IR spectra of **2-OTf** (black) and **3-OTf** (red). c) Characteristic cutout of the HR-ESI mass spectrum of **3-OTf** at room temperature, indicating the formation of the Cu_2OH complex. d) Cu K-edge XANES spectra of the precursor **2-OTf** (black) and the Cu_2OH complex **3-OTf** (red) at 293 K with enlarged pre-edge region. General remarks: UV/Vis: $l = 1$ cm.

a pre-edge feature at ~ 2 eV higher energies (~ 8980 eV) than Cu(II) (~ 8978 eV).^[32,33] Thus, the Cu(II) valence state of this complex is confirmed. Moreover, the XAS data of **3-OTf** are consistent with the crystal structure of **3-OTf** and the DFT-calculated Cu_2OH structure (Section S11.4).

2.1.8. EPR Spectroscopy

Apart from a small paramagnetic impurity ($g = 2.045$), which could already be observed in the Cu(I) complex **2-PF₆** at 77 K (Figure S89a, black), the Cu_2OH complex **3-PF₆** is EPR-silent (X-band, 77 K; Figure S89a, blue). This is due to an antiferromagnetic coupling of the Cu(II) centers in the Cu_2OH complex, as often observed for such systems.^[34–37]

2.2. Low-Temperature Oxygenation of **2-PF₆**

For the previously investigated dicopper complexes supported by the hexadentate ligands **bdpdz/bdptz**, it was shown that the formation of the Cu_2O species proceeds via homolytic bond

cleavage of a tetranuclear mixed-valent μ_4 -peroxo $[\text{Cu(I)}/\text{Cu(II)}]_2$ complex (Cu_4O_2) that can be detected at low temperature (183 K) upon reaction of the Cu(I) -precursor with O_2 .^[11] To check whether our new $\text{Cu}_2(\text{MO}8)$ system behaves similarly, **2-PF₆** was exposed to O_2 at 183 K, and the reaction was monitored by UV/Vis, rRaman, and XAS, as well as cryo-UHR-ESI mass spectrometry (cf Scheme 3, middle).

2.2.1. UV/Vis Spectrum

Upon reaction of **2-PF₆** with dioxygen at 183 K, the color of the solution changes from red to an intense darker red, going along with a change of the initial spectrum of the precursor (Figure 5a, black, $\lambda_{\text{max}} = 396$ nm and $\epsilon = 4700 \text{ M}^{-1}\text{cm}^{-1}$) to a product spectrum containing a band at 412 nm ($\epsilon = 2400 \text{ M}^{-1}\text{cm}^{-1}$) and a band at 625 nm ($\epsilon = 160 \text{ M}^{-1}\text{cm}^{-1}$) (Figure 5a, inset). These bands can be assigned as a $\pi^*(\text{OOH}) \rightarrow \text{Cu(II)}$ CT (412 nm) and a d-d transition (625 nm) of a μ -1,1-hydroperoxo dicopper(II) (Cu_2OOH) species **5**. Notably, similar absorption features around 400 nm and 600–650 nm have been observed for other Cu_2OOH complexes as well, whereas μ -1,2 peroxo dicopper complexes

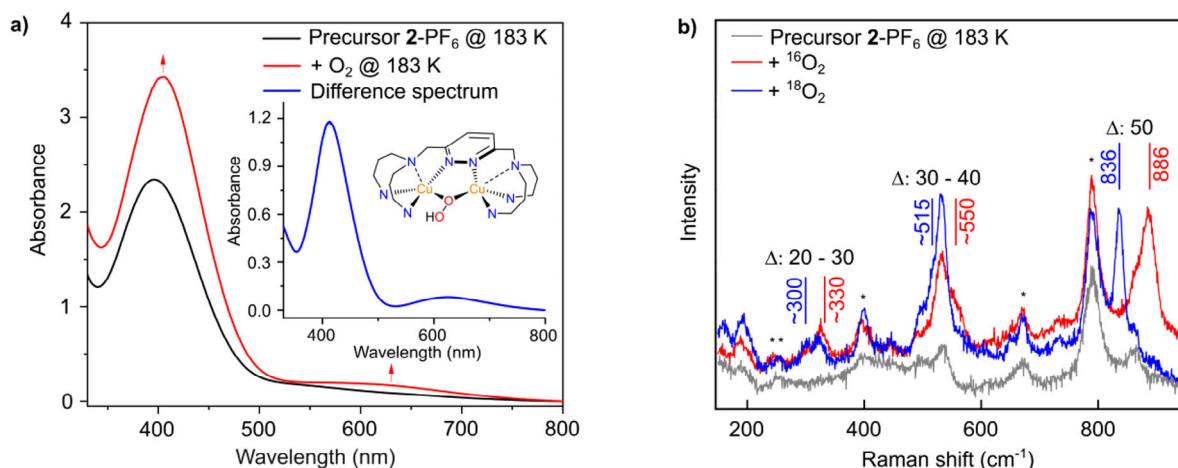


Figure 5. Identifying the μ -1,1-hydroperoxo dicopper(II) intermediate 5. a) Absorption spectra of an acetone solution of 2-PF₆ before (black) and upon reaction with O₂ (red) at 183 K. Inset: Difference Spectrum b) rR spectra of 2-PF₆ before (gray) and after the reaction with ¹⁶O₂ (red) and ¹⁸O₂ (blue) at 183 K. General remarks: UV/Vis: $l = 1$ cm. Raman: The asterisks mark solvent signals of acetone. The laser excitation wavelength was 420 nm.

give qualitatively different spectra.^[7,9,27,36,38–44] The proton of the hydroperoxido ligand probably originates from traces of H₂O in the solvent or from the solvent itself. To judge whether in principle a *trans* μ -1,2 dicopper (Cu₂O₂) species could form at low temperature, we also employed DFT. Geometry optimization led to a μ -1,2 peroxo structure (Figure S112) with a Cu-O-O-Cu torsion angle of 89°, similar to the pyrazolate-bridged system of Meyer et al.^[38] However, such a species would exhibit a two-band UV/Vis spectrum with an additional absorption band at around 500 nm.^[38] We therefore can exclude a Cu₂O₂ species resulting from low-temperature oxygenation of the MO8 system. Notably, electronic spectroscopy also excludes the formation of a Cu₄O₂ intermediate, which had been observed upon low-temperature oxygenation of the Cu(I) complexes supported by the **bdpdz**/**bdptz** ligands (see above). This marks an important difference between these systems and the new MO8 complex. Finally, warming of the Cu₂OOH complex of MO8 does not lead to a Cu₂O complex via O-O cleavage, as observed for the Cu₄O₂ species in the **bdpdz**/**bdptz** system. Rather, a thermal decay of the Cu₂OOH complex is observed (Figure S30).

2.2.2. rRaman

To further support formation of the Cu₂OOH complex, rR spectroscopy with an irradiation wavelength of 420 nm was employed. Upon reaction of 2-PF₆ with dioxygen (¹⁶O₂ and ¹⁸O₂) at 183 K, three isotope-sensitive peaks emerge at 886 cm⁻¹ ($\Delta = 50$ cm⁻¹), at around 550 cm⁻¹ ($\Delta = 30$ –40 cm⁻¹) and around 330 cm⁻¹ ($\Delta = 20$ –30 cm⁻¹; Figure 5b). DFT calculations performed for the Cu₂OOH complex predict a symmetric and an antisymmetric Cu-O stretching vibration at 282 cm⁻¹ ($\Delta = 10$ –30 cm⁻¹) and 495 cm⁻¹ ($\Delta = 2$ cm⁻¹), respectively. The O-O vibration is predicted to be at 936 cm⁻¹ ($\Delta = 51$ –68 cm⁻¹; Section S6.1). Calculations were performed without any coligands like acetone or acetonitrile; values with acetone or with acetonitrile can be found in Table S6. Correspondingly, the peak at 886 cm⁻¹

is attributed to the O-O stretch. Based on their frequencies, the observed modes around 550 cm⁻¹ and 330 cm⁻¹ are assigned to the antisymmetric and symmetric vibration of the Cu₂OOH species 5, respectively.

The vibrational frequencies and isotope shifts of the observed peaks are in good agreement with literature data for Cu₂OOH complexes.^[7,9,27,36,38–44] Specifically, the O-O stretch at ~ 890 cm⁻¹ rules out the formation of a μ -1,2 Cu₂O₂ complex, as such complexes exhibiting twisted Cu-O-O-Cu units (see above) have O-O stretching vibrations about 70–80 cm⁻¹ lower in frequency.^[7]

2.2.3. Cryo-UHR-ESI-MS

As a complement to the low-temperature spectroscopic data, cryo-UHR-ESI MS data were collected. Upon reaction of an acetone solution of 2-PF₆ with O₂ at 183 K, the mass spectrum shows a peak with an isotopic pattern and m/z value corresponding to a doubly positively charged [Cu₂O₂(MO8)]²⁺ species (calc. m/z 336.0754, obs. m/z 336.0922). This is superimposed by a mixed-valent μ -chlorido dicopper(I/II) species of 2-PF₆ (calc. m/z 337.5649, obs. m/z 337.5651; Section S9.1 / Figure S68) whereby the origin of the chloride is unknown. In the case of Cu₂OH complex 3, we have already observed that a Cu₂O complex was detectable under the conditions of mass spectrometry. It is therefore conceivable that the observed Cu₂O₂ species is formed by deprotonation of the Cu₂OOH complex 5 under the same conditions. Finally, we obtained a spectrum that is in excellent agreement with the calculated spectrum and isotopic distribution pattern of a doubly positively charged [Cu₂(MO8)O]²⁺ species [4]²⁺ (calc. m/z 328.0780, obs. m/z 328.0785; (Section S9.2 / Figure S70). This indicates that also a Cu₂OOH complex is partly converted to a Cu₂O complex in the gas phase. By contrast, a Cu₄O₂ complex could not be detected for 2-PF₆ in the MS experiment, in agreement with the UV/vis and Raman data. We assume that, due to the sterically more demanding ligand design of MO8 compared to **bdpdz**/**bdptz**, this intermediate

is not stable. DFT calculations support this hypothesis; that is, geometry optimization of a Cu_4O_2 starting structure leads to a unit of the dicopper(I) complex **2** moving away from the Cu_4O_2 core, leaving behind a μ -1,1-peroxo dicopper (Cu_2O_2) species (Section S12.1/ Figure S109).

2.2.4. XAS

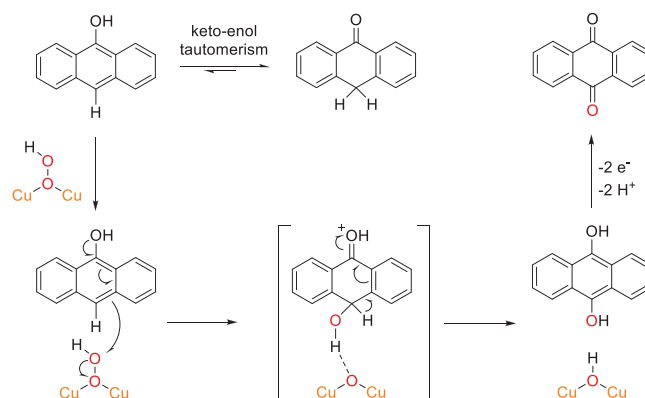
To characterize the oxidation state and structure of the species generated by the addition of oxygen to the precursor **2-PF₆** at ~ 190 K, XAS measurements were performed. They showed that upon addition of oxygen, Cu(I) was partially oxidized (Section S11.2, Figure S90). However, since the conversion to the oxidized species was not complete, structural analysis of this species could not be performed.

2.2.5. Reactivity of the Cu_2OOH Complex

The UV/Vis and Raman spectroscopic results presented above indicate that upon low-temperature oxygenation (183 K) of the $\text{Cu}_2(\text{MO8})$ system, a μ -1,1-hydroperoxo dicopper(II) intermediate (**5**) is formed (Scheme 3, middle). The ability of **5** to catalyze the monooxygenation of hydrocarbons was evaluated with 9,10-dihydroanthracene (DHA; BDE = 78 kcal mol⁻¹) and anthrone (AT; BDE = 76 kcal mol⁻¹). Upon addition of 5 equiv. of DHA to the Cu_2OOH complex of $\text{Cu}_2(\text{MO8})$, no reaction was observed. However, the reaction of **5-PF₆** and **5-OTf** with 5 equiv. of AT gave 9,10-anthraquinone (AQ) with a TON of 1.1 (for **5-PF₆**) and 1.0 (for **5-OTf**), corresponding to a stoichiometric conversion. Blind reactions were also performed using $[\text{Cu}(\text{NCMe})_4]\text{PF}_6$ or $[\text{Cu}(\text{NCMe})_4]\text{OTf}$ and O_2 instead of **2**, which led to a TON of 0.3 (for $[\text{Cu}(\text{NCMe})_4]\text{PF}_6$) and a TON of 0.4 (for $[\text{Cu}(\text{NCMe})_4]\text{OTf}$); that is, to poorer results compared to the activity of **5** (see Table S18).

Oxygen transfer to substrates by Cu_2OOH complexes has been described in the literature. For example, oxygen could be transferred stoichiometrically to PPh_3 or tetramethylene sulfide by a Cu_2OOH species, whereby $\text{O} = \text{PPh}_3$ or tetramethylene sulfoxide are formed.^[36,45] Furthermore, it was observed that in some ligand systems the Cu_2OOH species led to arene hydroxylation of the aromatic xylene backbone.^[40,46] The Cu_2OOH species of $\text{Cu}_2(\text{MO8})$ may behave similarly toward AT.

In solution, a keto-enol equilibrium between AT and 9-anthrol is present, depending on the solvent.^[47] (Scheme 4, top). The *para* position of the hydroxyl group in 9-anthrol is probably the most favorable for electrophilic attack by the Cu_2OOH species, since this position is activated by the OH group and the other positions are blocked by the neighboring benzene rings. Assuming that the reaction proceeds as an aromatic hydroxylation (cf Scheme 4, bottom), a Cu_2OH species would result that is inactive toward further oxygen transfer (see below).^[40] This would explain the fact that the reaction is stoichiometric under these conditions. Further oxidation of the anthrahydroquinone leads to AQ.



Scheme 4. Reactivity of the Cu_2OOH complex of **MO8** toward AT. In solution, AT is in equilibrium with the aromatic 9-anthrol via keto-enol tautomerism. Oxygenation through the Cu_2OOH species **5** could proceed via aromatic hydroxylation (see text).

2.3. Room Temperature Oxygenation of **2-PF₆**

2.3.1. UV/Vis

Upon oxygenation of a solution of the dicopper(I) complex **2-PF₆** in acetone at 293 K, a color change from red to an intense green is observed within 24 hours, going along with a change of the initial spectrum of the precursor (Figure 6a, black) to a product spectrum containing one shoulder at 360 nm ($\epsilon = 1900 \text{ M}^{-1}\text{cm}^{-1}$) and a band at 645 nm ($\epsilon = 200 \text{ M}^{-1}\text{cm}^{-1}$) (Figure 6a, red). Because the intense green color (Figure 6a, inset) has been associated with μ -oxo moieties in dicopper complexes,^[6,11,46] we initially assumed that a Cu_2O core is formed in our $\text{Cu}_2(\text{MO8})$ system as well. However, this hypothesis had to be abandoned upon closer examination. For simplicity, the room-temperature oxygenation product of **2** is therefore denoted as “green species” in the following (cf Scheme 3 top left).

To obtain further information, **2-PF₆** was also reacted with the common oxygen-atom transfer (OAT) reagent iodosobenzene (PhIO)^[6,11] in acetone at 263 K. In this case, the color changed from red to intense green within 2 hours, and a spectrum emerged (Figure 6b, violet) that was very similar to that obtained with O_2 , exhibiting one shoulder at 360 nm ($\epsilon = 1300 \text{ M}^{-1}\text{cm}^{-1}$) and a distinct absorption band at 651 nm ($\epsilon = 50 \text{ M}^{-1}\text{cm}^{-1}$). In addition, we investigated whether the same species can also be obtained using nitrous oxide (N_2O) as an OAT reagent.^[48] For this purpose, **2-PF₆** was reacted with N_2O for 48 hours at 308 K (Figure S33, red). Again, a color change from red to intense green occurred, and the resulting spectrum was found to be similar to that obtained for the reaction with O_2 and PhIO, exhibiting one shoulder at 355 nm ($\epsilon = 4800 \text{ M}^{-1}\text{cm}^{-1}$) and a distinct absorption band at 645 nm ($\epsilon = 90 \text{ M}^{-1}\text{cm}^{-1}$). It should be noted that the ratio of these two extinction coefficients differs depending on the oxygen reagent being used. While the reaction with PhIO is completed within 2 hours at 263 K, the reaction with O_2 takes 24 hours at 293 K and with N_2O 48 hours at 308 K. Therefore, the different ratios of the extinction coefficients might reflect differences in the completeness of the oxygenations. In any case,

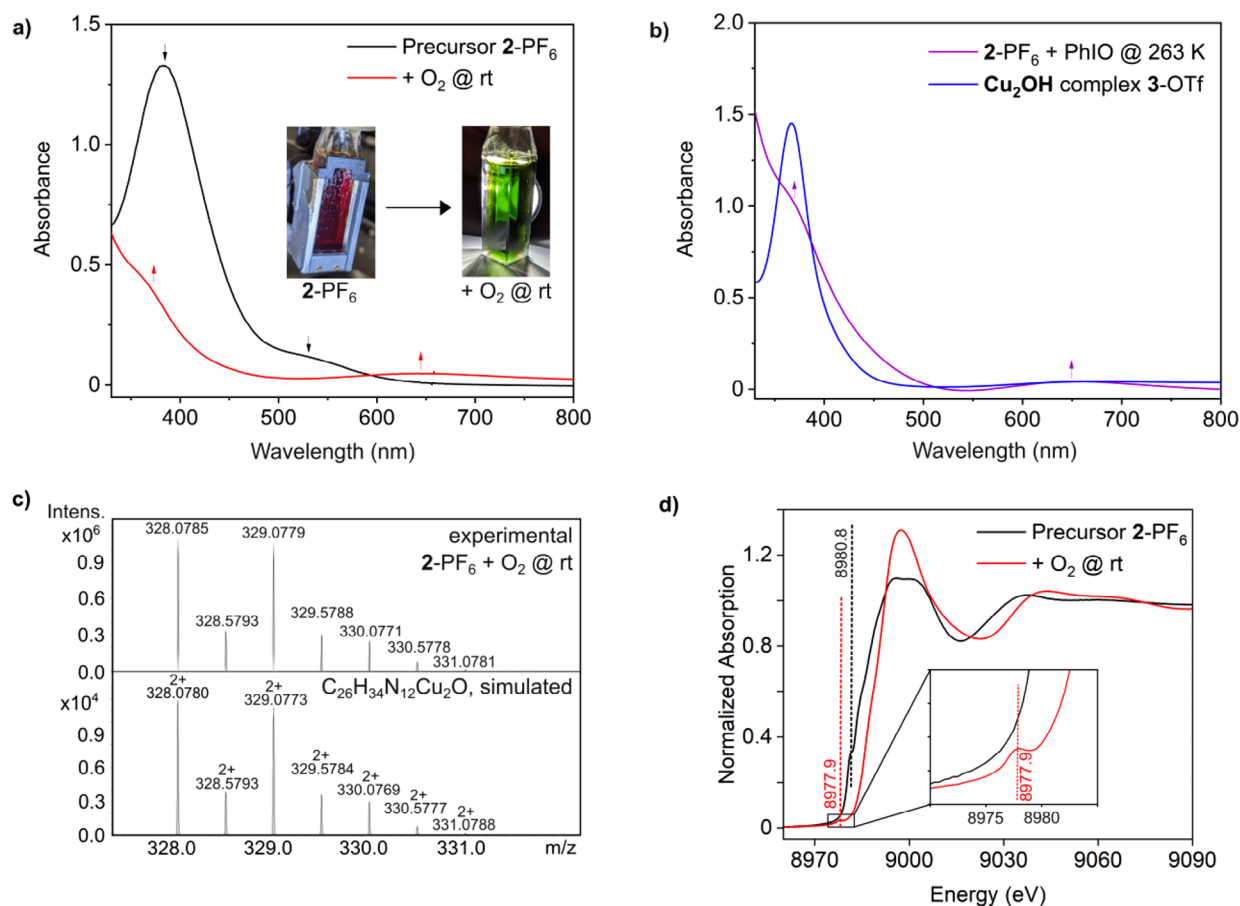


Figure 6. Reaction of 2-PF₆ with O₂ at room temperature. a) Absorption spectra of an acetone solution of 2-PF₆ before (black) and upon reaction with O₂ (red) at room temperature. b) The reaction of 2-PF₆ dissolved in acetone with an excess of PhIO (violet) at 263 K resulted in a green solution and comparable absorption features to the spectrum obtained after reaction with O₂ at room temperature. The spectrum of the Cu₂OH complex 3-OTf (blue) differs from the spectra of the room temperature oxygenation experiments. c) Characteristic cutout of the UHR-ESI mass spectrum obtained upon reaction of 2-PF₆ with ¹⁶O₂ at room temperature, showing the formation of the mono μ -oxo complex. The corresponding species is also detected in the experiment with ¹⁸O₂ and upon reaction with PhIO at 263 K and N₂O at 293 K (see Section S9, Figures S73–S77). d) Cu K-edge XANES spectra of the precursor 2-PF₆ before (black line, Cu(I)) and after the reaction with dioxygen at 293 K (red line) with enlarged pre-edge region. General remarks: UV/Vis: l = 1 cm.

however, the obtained spectra are different from that of the Cu₂OH complex **3** (Figure 6b).

Absorption features around 600 nm have been observed for and associated with Cu₂O complexes.^[6,11,12,15,35,49] Compared with the Cu₂(bdpdz/bdptz) systems studied earlier,^[11] however, significantly lower ϵ values are observed for the MO8 complex. Moreover, in the case of the former systems^[11] the Cu₂O intermediates were only stable up to -35°C whereas the “green species” is stable at room temperature.

2.3.2. rRaman

In order to check whether the “green species” corresponds to a Cu₂O complex or not, rR spectroscopy was employed, using an irradiation wavelength of 360 nm. However, upon reaction of 2-PF₆ with dioxygen at room temperature, no isotope-sensitive peak around 600–630 cm⁻¹,^[4,6,10–12,15,50] as expected for a Cu₂O species, could be detected. Instead, a spectrum was obtained that is consistent with the Cu(I) precursor (Figure S36). Nevertheless, the UV/Vis spectra shown in Figure 6a,b indicate that the species obtained after oxygenation is not the precursor com-

plex, and the green color of this intermediate could also be observed when recording the rR-data. We thus conclude that the “green species” is photolabile under the conditions of the Raman experiment.

2.3.3. IR Spectroscopy

As Raman spectroscopy proved to be ineffective, IR spectroscopy was employed to obtain information regarding the nature of the “green species.” Interestingly, the obtained spectrum (Figure S47) shows two bands in the frequency range of O–H stretches, suggesting the presence of two hydroxo ligands. Based on DFT, a μ -hydroxo hydroxo complex Cu₂(μ -OH)OH (**6**) (structure cf. Figure S51) exhibits two O–H bands in the IR spectrum with the observed splitting (Table S8). Such a species could result from hydration of a mono μ -oxo dicopper (Cu₂O) complex formed initially by oxygenation of the Cu(I)₂MO8 complex **2**. Alternatively, it could derive from the reaction of an initially formed Cu₂OOH complex with a residual Cu(I) complex. Importantly, EXAFS data do not exclude the possibility that the green species corresponds to **6** (see below).

2.3.4. Cryo-UHR-ESI-MS

Reaction of 2-PF₆ with O₂ at 293 K provides the mass spectrum shown in Figure 6c, which is in excellent agreement with the calculated spectrum and isotopic distribution pattern of a doubly positively charged Cu₂O species [4]²⁺ (calc. *m/z* 328.0780, obs. *m/z* 328.0785; similar data obtained with PhIO and N₂O are shown in Sections S9.3, S9.4). Upon reaction with ¹⁸O₂, the peak shifts by one mass unit to *m/z* 329.0781, as expected (calc. *m/z* 329.0801, Figure S73). It should be noted that acetonitrile had to be used as a solvent instead of acetone to detect the Cu₂¹⁸O species. In acetone, even when using ¹⁸O₂, only the Cu₂¹⁶O complex could be detected (see Section S9.2). We ascribe this to the exchange of ¹⁸O with the solvent. Moreover, we observed a mass spectrum that is in excellent agreement with a doubly positively charged Cu₂O₂ species [Cu₂(MO8) (O₂)]²⁺ (calc. *m/z* 336.0754, obs. *m/z* 336.0759; Section S9.6).

To conclude, cryo-UHR ESI-MS does provide evidence for the formation of a Cu₂O complex (4) resulting from room-temperature oxygenation of the Cu(I)₂MO8 precursor 2. However, as 4 has also been observed by ESI-MS under conditions where it clearly is *not* present in homogeneous solution (see above), we cannot take this result as proof for the contention that the 'green species' corresponds to 4. If the 'green species' instead corresponds to the dihydroxo complex 6, as suggested by IR (see above), the Cu₂O species observed by MS might derive from dehydration of 6 in the gas phase.

2.3.5. XAS

Upon oxygenation of the copper(I) precursor (2-PF₆) with O₂ at room temperature for 24 hours, E_{1/2} in the Cu K-edge XANES spectra shifts to higher energy by 3.9 eV (8983.4 eV to 8987.3 eV), reflecting the transition from Cu(I) to Cu(II). Concomitantly, a pre-edge feature appears at 8977.9 eV, reflecting the emergence of Cu(II) character (Figure 6d).^[29,30,32] However, of several different models tested (Figure S91), EXAFS is not pointing to one model with certainty. In particular, it is not possible by detailed EXAFS analysis to associate a Cu₂O structure to the Cu(II) species formed (Section S11.2).

2.3.6. EPR Spectroscopy

In contrast to the Cu₂OH complex 3-PF₆, a frozen solution of the "green species" exhibits an EPR signal with *g* = 2.092 (Figure S89b) in the X-band EPR spectrum measured at 77 K, which suggests the presence of Cu(II).^[51] The signal also indicates a weaker antiferromagnetic coupling of the Cu(II) centers for the "green species" compared to the Cu₂OH complex 3-PF₆. The reason for this could be a geometric distortion of the system caused by the second hydroxido ligand that is present in the dihydroxo complex 6 (see above and Figure S51). Notably, the observation of an EPR signal is also incompatible with the presence of a Cu₂O species, which exhibits strong antiferromagnetic coupling.^[11]

2.4. Attempt to Generate the Mono μ -oxo Dicopper Complex with dimethyldioxirane (DMDO) at Low Temperature

Since generation of a Cu₂O species with our Cu₂(MO8) system at room temperature could not be demonstrated so far, we tried in the next step to generate a Cu₂O species at low temperatures using the highly reactive oxygen atom transfer reagent DMDO.^[52] We anticipated that the reaction of 2-PF₆ with DMDO leads to the Cu₂O complex 4-PF₆. The potential higher stability of a Cu₂O species at low temperature could facilitate spectroscopic characterization of this complex. UV/Vis spectroscopy, Cryo-UHR-ESI-MS, and XAS were employed to investigate this reaction (Scheme 3, right).

2.4.1. UV/Vis

Analogous to the reaction with oxygen at room temperature, the solution of 2-PF₆ changed its color to green after an addition of DMDO at 193 K. The UV/Vis spectrum revealed an absorption band at 368 nm (ϵ = 4500 M⁻¹cm⁻¹) and a band at 660 nm (ϵ = 135 M⁻¹cm⁻¹) (Figure 7a). The UV/Vis bands are in the same position as in the experiments with O₂, PhIO, and N₂O, which indicates that the same copper-oxygen intermediate could have been generated in this experiment. In the case of oxygenation with DMDO, however, the bands are more pronounced, possibly due to a better stabilization of this species at the lower temperature. Warming up to room temperature led to a decrease of both bands in the UV/Vis spectrum and to a fading of the green color of the solution, indicating a decay of the complex.

2.4.2. Cryo-UHR-ESI-MS

To gain further information in the generated copper-oxygen intermediate, Cryo-UHR-ESI-MS measurements were performed. After the reaction of 2-PF₆ with DMDO at 193 K, a mass spectrum (Figure 7c) was obtained which, as in the experiments with O₂, PhIO, and N₂O, corresponds to the calculated spectrum and isotopic distribution pattern of the Cu₂O species [4]²⁺ (calc. *m/z* 328.0780, obs. *m/z* 328.0772). As pointed out before, however, this species may result from deprotonation of the Cu₂OH complex 3 the presence of which in homogeneous solution is indicated by XAS (see below). The addition of a large excess of DMDO or the addition of DMDO at rt resulted in a relatively smaller peak of the Cu₂O species [4]²⁺ as well as more decomposition products, probably due to the high reactivity of this OAT (Figure S87).

2.4.3. XAS

2-PF₆ was also reacted with DMDO at 193 K, and the reaction was monitored by XAS. Upon oxygenation of 2-PF₆ with DMDO, the intensity of the shoulder at 8981.5 eV in the Cu K-edge XANES spectrum is strongly reduced, resulting in the shift of the edge position E_{1/2} to higher energy by 3.6 eV (8983.9 eV to 8987.5 eV). A pre-edge feature appears at 8977.5 eV (Figure 7b, S92). Thus, we

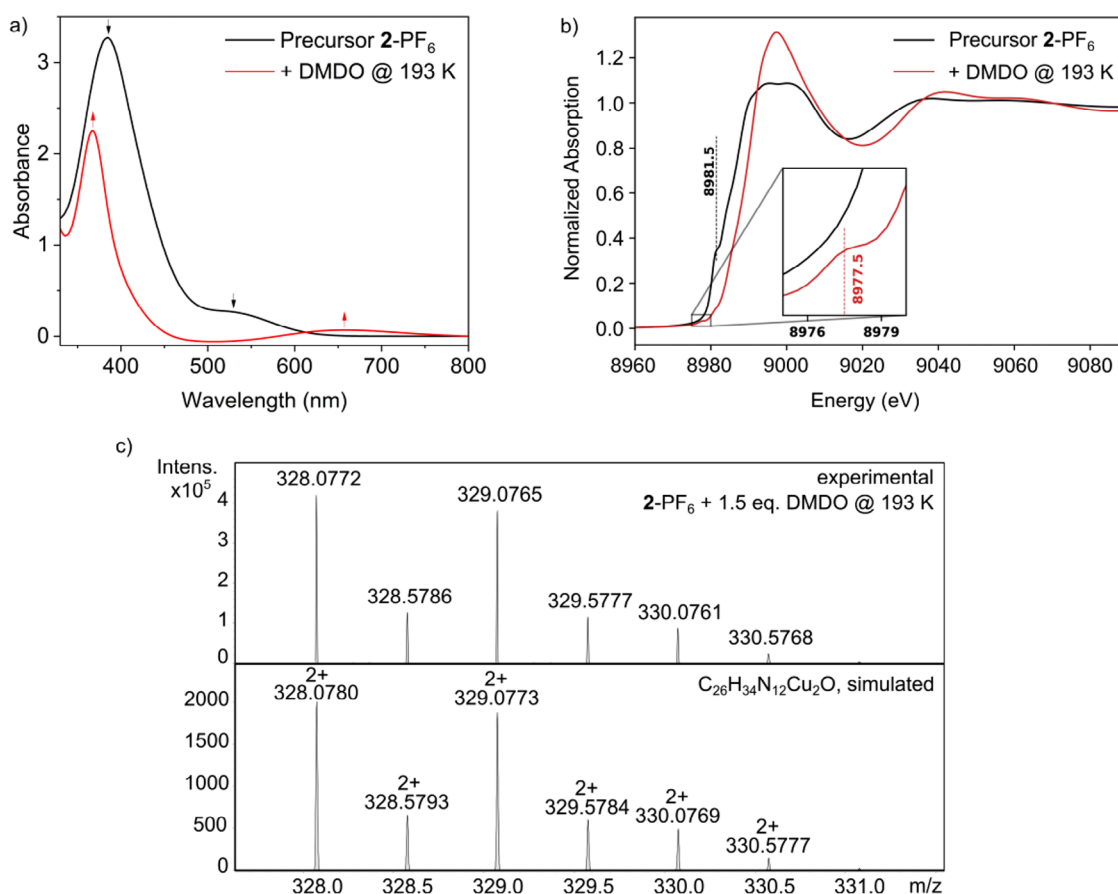


Figure 7. Reaction of 2- PF_6 with DMDO at 193 K. a) UV/Vis spectrum obtained after reaction of 2- PF_6 with DMDO at 193 K. The spectrum shows comparable features to the experiments with O_2 (at rt), PhIO, and N_2O . b) Cu K-edge XANES spectra of the precursor 2- PF_6 before (black line, Cu(I)) and after the reaction with DMDO at 193 K (red line) with enlarged pre-edge region. c) Characteristic cutout of the UHR-ESI mass spectrum obtained upon reaction of 2- PF_6 with DMDO at 193 K, indicating the formation of the mono- μ -oxo complex.

can identify the oxidized species as a Cu(II) complex. Comparison of spectra obtained by oxidation of 2- PF_6 with oxygen and with DMDO is shown in Figure S94.

Further structural insights are provided by extended EXAFS analysis. Comparison of the fit results for different models is shown in Section S11.3 (Figures S95–S99). It follows that the copper-oxygen intermediate that best fits the EXAFS data is the crystal structure of the μ -hydroxo dicopper(II) (Cu_2OH) species (3). Specifically, for the Cu_2O species, a copper-oxygen distance of $\text{Cu}-\text{O} = 1.89 \text{ \AA}$ (about the same value as determined for the Cu_2O intermediate of the bdpdz/bdptz system)^[11] and $\text{Cu}-\text{N}_{\text{Amine}}$ distances of 2.29 \AA and 2.36 \AA are calculated. For the Cu_2OH complex 3, the corresponding values are $\text{Cu}-\text{O} = 1.95 \text{ \AA}$; $\text{Cu}-\text{N}_{\text{Amine}} = 2.17 \text{ \AA}$ and 2.18 \AA (RI-PBE-D3(BJ)/def2-SVP^[23,24]). Notably, there is also evidence for a Cu_2OH species in the Cryo-UHR-ESI-MS (see Figure S79), but the intensity of this species is much smaller than that of the Cu_2O complex.

In summary, the spectroscopic data indicate that targeted oxygen transfer to 2- PF_6 is possible with DMDO at low temperatures, but the characterization with XAS rather indicates the presence of a Cu_2OH complex that may result from protonation of a Cu_2O complex formed initially (cf Scheme 3, right).

2.5. Attempt to Generate the Mono μ -oxo Dicopper Complex by Deprotonation of the μ -Hydroxo Complex

It has been shown in the literature that a Cu_2O species can be formed by deprotonation of a Cu_2OH complex.^[53] Therefore, we wanted to investigate if the Cu_2OH complex 3 can be deprotonated with the base diazabicycloundecene (DBU) to generate a Cu_2O species (Scheme 3, right). The reaction was monitored using UV/Vis spectroscopy and XAS.

2.5.1. UV/Vis

For the deprotonation experiment, a solution of 3-OTf in acetone was cooled to 223 K, and 1.5 eq. DBU was added. The 0.5 mM solution used for low-temperature UV/Vis spectroscopy changed its color from green to orange within 90 minutes after adding DBU and warming to 233 K. This resulted in a UV/Vis spectrum with bands at 370 nm ($\epsilon = 5300 \text{ M}^{-1}\text{cm}^{-1}$), 550 nm ($\epsilon = 210 \text{ M}^{-1}\text{cm}^{-1}$), 680 nm ($\epsilon = 125 \text{ M}^{-1}\text{cm}^{-1}$) and 860 nm ($\epsilon = 90 \text{ M}^{-1}\text{cm}^{-1}$). The color of the solution and the shape of the spectrum are similar to Cu(I) complex 2.

Furthermore, the band at 680 nm, which indicates a Cu(II) d-d transition, has decreased significantly (Figure 8a, red). These

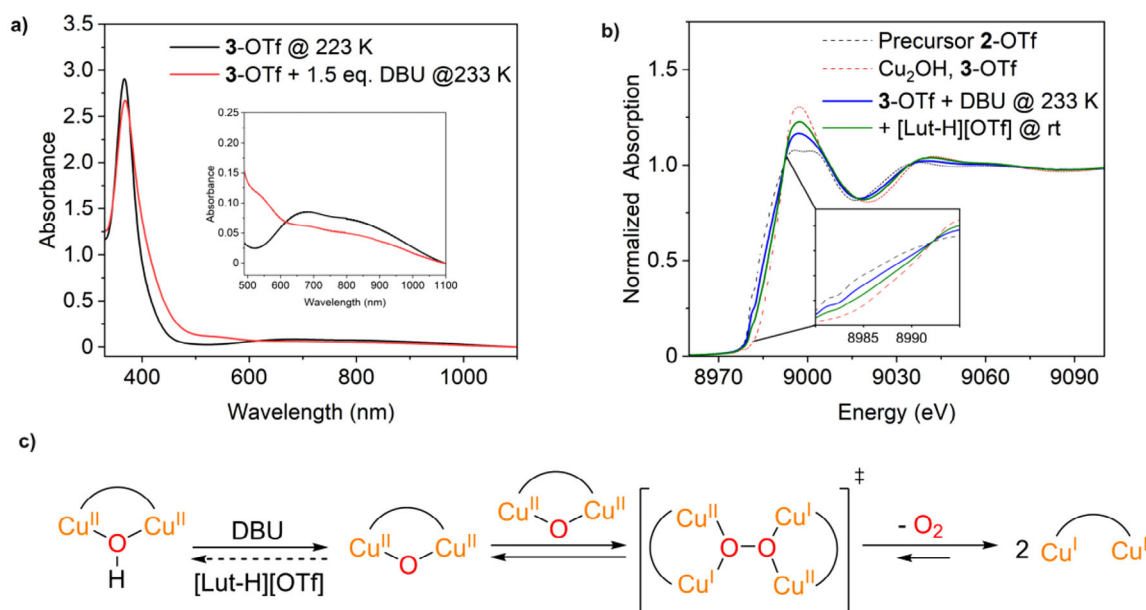


Figure 8. Deprotonation of the Cu_2OH species **3**. a) UV/Vis spectra of the Cu_2OH complex **3-OTf** before (black) and after deprotonation with DBU (red). b) EXAFS spectra of the Cu(I) complex **2-OTf** (black) and Cu_2OH complex **3-OTf** (red) from Figure 4 and spectra obtained after the deprotonation with DBU at 233 K (blue) and after addition of $[\text{Lut-H}][\text{OTf}]$ at rt (green). c) Proposed reaction sequence: At first the deprotonation of the Cu_2OH complex might lead to a Cu_2O species. However, when two Cu_2O cores interact, an O-O bond might be formed and generate a Cu_4O_2 transition state, which immediately releases O_2 .

findings suggest that a Cu(I) complex is formed when DBU is added to the Cu_2OH species. We then checked whether the observed reaction was reversible by adding an acid. For this purpose we used 2,6-lutidinium triflate ($[\text{Lut-H}][\text{OTf}]$). After the addition of 1.5 eq. $[\text{Lut-H}][\text{OTf}]$ and warming to room temperature, the initial spectrum of Cu_2OH complex **3** could only be partially restored (Figure S25). The color of the solution was paler than the Cu_2OH complex before the addition of DBU and the bands were not as intense, which indicates that irreversible processes take place during deprotonation.

2.5.2. XAS

The deprotonation of the Cu_2OH complex was also monitored using XAS with a 16 mM solution of **3-OTf** in acetone. To this end, 1.5 eq. DBU was added to an acetone solution of **3-OTf** at 233 K, and the reaction mixture was stirred for 2 hours. The XAS measurement showed that a large part of the Cu(II) complex was converted to Cu(I) after reaction with DBU, which supports the observed results from the low-temperature UV/Vis spectroscopy. Linear combination fit (LCF) of the XANES spectrum confirmed that the resulting solution consisted of **2-OTf** (64%) and **3-OTf** (36%) (Figure 8b, blue, Figure S103). As in the UV/Vis experiment, the addition of 1.5 eq. $[\text{Lut-H}][\text{OTf}]$ only partially restored the Cu(II) species (according to LCF, the resulting solution consisted of 35% **2-OTf** and 65% **3-OTf**) (Figure 8b, green, Figure S104). The reaction of the Cu_2OH complex with DBU could initially form a Cu_2O complex. Reaction between two Cu_2O units may form an O-O bond and a transient Cu_4O_2 species. Subsequent release of O_2 could then lead to a Cu(I) complex (Figure 8c). Notably, this reaction sequence corresponds to the reversal of the reaction of

the former **bdpdz/bdptz** system with O_2 , generating mono μ -oxo dicopper complexes from the Cu(I) precursor and O_2 .^[11] In summary, this experiment indicates that a Cu_2O species is unstable in the **MO8** system as it decays to Cu(I) and O_2 .

2.6. Reactivity of the "Green Species"

In the last step, we investigated the ability of the "green species" to catalyze the monooxygenation of hydrocarbons. This was evaluated with a range of aliphatic substrates exhibiting bond dissociation energies (BDEs) from 75 to 82 kcal mol⁻¹; that is, 9H-xanthene (XEN; BDE = 75 kcal mol⁻¹),^[54,55] 10H-anthracen-9-one also denoted as (AT; BDE = 76 kcal mol⁻¹),^[56] 9,10-dihydroanthracene (DHA; BDE = 78 kcal mol⁻¹)^[34,55,57] and diphenylmethane (DPM; BDE = 82 kcal mol⁻¹)^[54] at room temperature (Table 1 and Section S13.1). Specifically, oxygenation of 10 equiv. of xanthene with the "green species" resulted in no conversion to 9H-xanthene-9-one (XON) at all. A negative result was also obtained when the conversion of DHA to 9,10-AQ was tested; that is, upon addition of 10 equiv. of DHA to the "green species," no reaction was observed (Table 1). These results already indicated that the monooxygenation activity of the $\text{Cu}_2(\text{MO8})$ system is lower than that of the original **bdpdz/bdptz** complexes. Correspondingly, no conversion to benzophenone (Ph_2CO) was observed upon addition of 10 equiv. of diphenylmethane to the "green species."

Finally, AT was investigated as a substrate. Here we found that oxygenation of 10 equiv. of AT leads to 9,10-AQ with a TON of 9 (~90% conversion) (Table 1). This clearly demonstrates that **2-PF₆/OTf** is principally able to convert aliphatic substrates like

Table 1. Catalytic activities for the oxygenation of hydrocarbons. Overview of the catalytic activities of the new model system $\text{Cu}_2(\text{MO8})$ after oxygenation at room temperature compared to the activities of our initial systems $[\text{Cu}_2(\text{bdpdz})(\text{NCMe})_2]\text{X}_2$ and $[\text{Cu}_2(\text{bdptz})(\text{NCMe})_2]\text{X}_2$ toward various substrates.

BDE/kcal mol ⁻¹	Substrate → Product	TON ^[a] bdpdz/bdptz	TON ^[b] 2-PF ₆ /-OTf
75	XEN→XON	3/2 ^[11]	0/0
76	AT→AQ	2/2	9/9
78	DHA→AQ ^[c]	3/5 ^[11]	0/0
82	DPM→Ph ₂ CO	2/2 ^[11]	0/0

General Remarks: Conditions: 1 equiv. of **2** and 10 equiv. of 9*H*-xanthene (XEN), 10*H*-anthracen-9-one (anthrone /AT), 9,10-dihydroanthracene (DHA), or 50 equiv. of diphenylmethane (DPM) were applied (cf. Section [S13.1](#)). Blind reactions were also performed using [Cu(NCMe)₄]PF₆ or [Cu(NCMe)₄]OTf and O₂ instead of **2**. All control experiments lead to poorer results compared to the activity with **2** (see Table [S17](#)). For abbreviations, see text.

[a] The Cu_2O complex was reacted at -35°C with the substrate for 2 hours and additional an 2 hours at room temperature.^[11]

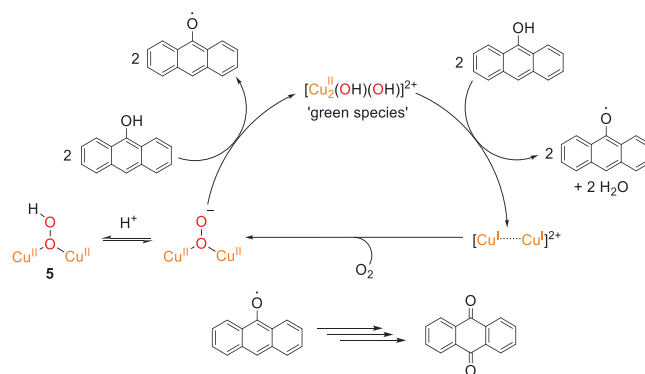
^[b] Conditions for the Cu₂(M08) model systems: +35 °C, 2 hours of O₂ bubbling in the beginning; total time of the reaction: 24 hours.

[c] 10 equiv. of DHA were used, representing a 20-fold excess of substrate. The given TON refers to the initially formed disecundary alcohol and does not include the subsequent oxidation.

AT to the corresponding ketones after oxygenation at room temperature, although its activity is much lower than that of the original **bdpdz**/**bdptz** system.^[11] It should be mentioned that AT is already partially oxidized in solution with O₂ to AQ, but only to a very small extent (6% at rt (see Table S17).

As indicated above (Scheme 4), AT is subject to a keto-enol tautomerism. The resulting enol (9-anthrol) has a lower BDE (O-H) of 72 kcal mol^{-1} [47,56] than the keto form (BDE (C-H) = 76 kcal mol^{-1} [47,56]), which could enable a reaction via an initial O-H abstraction (Scheme 4, left). This would also explain why no reaction is observed for 2-PF₆/OTf with xanthene, although its BDE (C-H) is lower than that of AT (see Table 1). Thus, starting from a **Cu₂(μ-OH)OH** species (6), two anthroxyl radicals may be generated via H-atom abstraction from anthrol, whereby a dicopper(I) complex is formed and water is eliminated. The anthroxyl radical might then react with atmospheric O₂ to form AQ. The Cu(I) complex could react with O₂ to form a μ-1,1 peroxo complex, which, by two-electron reduction from further anthrol molecules, converts to **6**, thus closing the catalytic cycle (Scheme 5). To compare this result with our former **Cu₂O** models, the activities of the **bdpdz** and **bdptz** systems toward the conversion of AT to AQ were determined as well. Interestingly, employing 10 equiv. of AT led to a TON of 2; that is, a *lower* yield than obtained with the **Cu₂(MO8)** system.

For comparison, we also investigated the reaction of the **Cu₂OH** complex **3-OTf** toward AT. The reaction was carried out at room temperature for 24 hours in analogy to the experiments with the “green species.” In a first attempt, the reaction was carried out under an inert atmosphere and in a second attempt, with an O₂-saturated solution (under the same conditions as the “green species.”) Under an inert atmosphere, only 0.1 eq. of the substrate was converted to AQ. In the O₂-saturated solu-



Scheme 5. Reactivity of the “green species” of MO8 toward AT. At room temperature an initially formed Cu_2O species might form a $\text{Cu}_2(\text{OH})\text{OH}$ complex which generates an anthroxyl radical via O-H abstraction of anthrol. AQ could then be formed by a further reaction of the anthroxyl radical with atmospheric O_2 .

tion 0.6 eq. of AQ were formed, similar to the reactivity of the $[\text{Cu}(\text{NCMe})_4]\text{OTf}$ precursor toward AT (see Table S19). The reactivity of the Cu_2OH complex **3-OTf** toward AT thus is significantly lower than observed for the Cu_2OOH complex **5** and the “green species.”

In conclusion, the Cu₂(MO8) system shows weaker C-H activation than our earlier model systems based on the ligands **bdpdz** and **bdptz**.^[11] However, it is capable of almost quantitative conversion of AT to AQ (TON = 9 for 10 equivalents), whereas the corresponding reaction catalyzed by **bdpdz** or **bdptz** only leads to a TON of 2.

3. Conclusion

Herein the synthesis of a new dinuclear Cu-monooxygenase model system based on the octadentate ligand **MO8** was described. Compared to our previous systems, which were based on the hexadentate ligands **bdpdz** and **bdptz**, no additional coligands coordinate to copper in the Cu(I) complex, which could be shown by the crystal structure of **2**-PF₆. Depending on the oxygenation conditions, different copper-oxygen intermediates are generated. In contrast to the **bdpdz/bdptz** system, the reaction of **2**-PF₆ with O₂ at 183 K does not lead to a **Cu₄O₂** complex. DFT calculations suggest that such a tetranuclear core is not stable in the Cu₂(**MO8**) system due to steric reasons. Instead, the spectroscopic data reveal the formation of a **Cu₂OOH** complex. A reactivity study of **Cu₂OOH** toward aliphatic hydrocarbons showed that (AT, 76 kcal mol⁻¹) is stoichiometrically converted to AQ.

Oxygenation of 2-PF₆ with O₂ at room temperature (or PhIO at 263 K, or N₂O at 308 K) generates a solution containing the “green species,” which we initially assumed to be a Cu₂O complex. This hypothesis could not be verified spectroscopically, in contrast to the **bdpdz** and **bdptz** systems investigated earlier.^[1] Notably, the IR spectrum of the “green species” shows two bands in the typical frequency range of O-H stretching vibrations, which could be due to a μ -hydroxo/hydroxo (Cu₂(μ -OH)OH) complex. This assumption was supported by DFT calculations,

and an EXAFS analysis also indicates that this might be a possibility.

The reactivity of the “green species” toward monooxygenation of aliphatic hydrocarbons was investigated with various substrates exhibiting BDEs from 75 to 82 kcal mol^{−1} at room temperature. The system was only able to convert the substrate AT to AQ, but with an almost quantitative yield. Overall, however, the monooxygenase activity of the **MO8** system is distinctly lower than that of the **bdpdz/bdptz** systems forming **Cu₂O** intermediates upon oxygenation.

Nevertheless, an attempt was made to generate, stabilize, and characterize a **Cu₂O** species at low temperatures, using the highly reactive OAT reagent DMDO. While UV/Vis and Cryo-UHR-ESI-MS support the formation of a **Cu₂O** species, XAS data are rather compatible with the presence of a **Cu₂OH** species. This complex was synthesized independently and employed for an attempt to generate the **Cu₂O** complex by deprotonation with diazabicycloundecene (DBU). The UV/Vis and XAS data, however, revealed that a Cu(I) complex is formed after the addition of DBU. Thus, deprotonation might initially lead to a **Cu₂O** species, which, however, decays to Cu(I) and O₂.

In contrast to the **bdpdz/bdptz** systems investigated earlier, it thus appears that the **Cu₂O** species of the **MO8** system is unstable in two ways: in the presence of base (i.e., when protons are absent), it decays into Cu(I) and O₂. In the presence of H⁺ (probably deriving from water), it either gets protonated, leading to a **Cu₂OH** complex, or even hydrated, leading to a dihydroxo complex, supposedly a **Cu₂(μ-OH)OH** species. This reflects an increased Brønsted basicity of the **Cu₂O** core with respect to the **bdpdz/bdptz** systems, which probably derives from the octadentate constitution of the **MO8** ligand, providing two nitrogen donors in *trans*-position to the μ-oxo unit. In the hexadentate **bdpdz/bdptz** systems, by contrast, these additional nitrogen atoms were absent, giving rise to a more electrophilic character of the **Cu₂O** core. These results establish an important structure-function correlation in copper-oxygen chemistry regarding the formation and stability of the rare and much sought-after mono μ-oxo dicopper cores.

Although we found that the targeted **Cu₂O** core cannot be stabilized in the **MO8** system, access to other reactive copper-oxygen species is possible. This is evidenced by catalytic conversion of the organic substrate AT to AQ that does not depend upon a mono μ-oxo dicopper intermediate.

Acknowledgments

The authors thank CAU Kiel for support of this research. Moreover, parts of this research were carried out at beamline P65 at the PETRA III storage ring at DESY, a member of the Helmholtz Association. We thank Edmund Welter, Sergiu Levenco and Marlene Vogt for their support at beamline P65. We also thank Kai Uwe Clausen and Tobias Engesser for IR spectroscopic measurements. We are grateful to Lina Liers and Sebastian Mangelsen for the measurement and interpretation of powder diffractograms. We would like to thank Laura Senft for the measurements of

Cryo-UHR-ESI mass spectra. We further thank Melissa Teubner for her help on the resonance Raman spectroscopy. M.N. is grateful to Aleksej Kuzmin for his guidance on using the EvAX software and for his valuable feedback on the EXAFS analysis. B. G.-L. gratefully acknowledges the Bundesministerium für Bildung und Forschung (BMBF) project 05K19GU5 for funding. S. B. gratefully acknowledges the Deutsche Forschungsgemeinschaft (DFG) for financial support under project RU 773/8-1.

Open access funding enabled and organized by Projekt DEAL.

Conflict of Interests

The authors declare no conflict of interest.

Data Availability Statement

The data that support the findings of this study are available in the supplementary material of this article.

Keywords: catalysis · copper · EXAFS spectroscopy · metalloenzymes · oxygenation

- [1] a) R. Trammell, K. Rajabimoghadam, I. Garcia-Bosch, *Chem. Rev.* **2019**, *119*, 2954; b) T. Newhouse, P. S. Baran, *Angew. Chem. Int. Ed.* **2011**, *50*, 3362; c) H. Sterckx, B. Morel, B. U. W. Maes, *Angew. Chem. Int. Ed.* **2019**, *58*, 7946; d) V. C.-C. Wang, S. Maji, P. P.-Y. Chen, H. K. Lee, S. S.-F. Yu, S. I. Chan, *Chem. Rev.* **2017**, *117*, 8574; e) C. Gawlig, S. Schindler, S. Becker, *Eur. J. Inorg. Chem.* **2020**, *2020*, 2448; f) C. Noß, R. Göttlich, S. Schindler, *Chem. Eur. J.* **2023**, *29*, e202301142.
- [2] C. W. Koo, A. C. Rosenzweig, *Chem. Soc. Rev.* **2021**, *50*, 3424.
- [3] a) R. B. Jackson, E. I. Solomon, J. G. Canadell, M. Cargnello, C. B. Field, *Nat. Sustain.* **2019**, *2*, 436; b) R. Peifer, L. Müller, S. Hoof, F. Beckmann, B. Cula, C. Limberg, *Z. Anorg. Allg. Chem.* **2021**, *647*, 1789.
- [4] J. S. Woertink, P. J. Smeets, M. H. Groothaert, M. A. Vance, B. F. Sels, R. A. Schoonheydt, E. I. Solomon, *Proc. Natl. Acad. Sci. USA* **2009**, *106*, 18908.
- [5] B. E. R. Snyder, M. L. Bols, R. A. Schoonheydt, B. F. Sels, E. I. Solomon, *Chem. Rev.* **2018**, *118*, 2718.
- [6] P. Haack, C. Limberg, *Angew. Chem. Int. Ed.* **2014**, *53*, 4282.
- [7] C. E. Elwell, N. L. Gagnon, B. D. Neisen, D. Dhar, A. D. Spaeth, G. M. Yee, W. B. Tolman, *Chem. Rev.* **2017**, *117*, 2059.
- [8] a) W. Keown, J. B. Gary, T. D. P. Stack, *J. Biol. Inorg. Chem.* **2017**, *22*, 289; b) E. I. Solomon, J. W. Ginsbach, D. E. Heppner, M. T. Kieber-Emmons, C. H. Kjaergaard, P. J. Smeets, L. Tian, J. S. Woertink, *Faraday Discuss.* **2011**, *148*, 11; discussion 97–108; c) S. Yelin, C. Limberg, *Catal. Lett.* **2020**, *150*, 1–11; d) M. Costas, A. Company, *Eur. J. Inorg. Chem.* **2022**, *2022*; e) J. de Tovar, R. Leblay, Y. Wang, L. Wojcik, A. Thibon-Pourret, M. Réglier, A. J. Simaan, N. Le Poul, C. Belle, *Chem. Sci.* **2024**, *15*, 10308.
- [9] L. M. Mirica, X. Ottenwaelde, T. D. P. Stack, *Chem. Rev.* **2004**, *104*, 1013.
- [10] M. Réglier, C. Jorand, B. Waegell, *Chem. Soc. Chem. Commun.* **1990**, 1752.
- [11] R. Jurgeleit, B. Grimm-Lebsanft, B. M. Flöser, M. Teubner, S. Buchenau, L. Senft, J. Hoffmann, M. Naumova, C. Näther, I. Ivanović-Burmazović, M. Rübhausen, F. Tuczek, *Angew. Chem. Int. Ed.* **2021**, *60*, 14154.
- [12] P. Haack, A. Kärger, C. Greco, J. Dokic, B. Braun, F. F. Pfaff, S. Mebs, K. Ray, C. Limberg, *J. Am. Chem. Soc.* **2013**, *135*, 16148.
- [13] R. Jurgeleit, B. Grimm-Lebsanft, M. Rübhausen, F. Tuczek, *Desy Photon Sci* **2021**, *2021*, 34.
- [14] a) A. Petrillo, A. Hoffmann, J. Becker, S. Herres-Pawlis, S. Schindler, *Eur. J. Inorg. Chem.* **2022**, *2022*, e202100970; b) M. Paul, A. Hoffmann, S. Herres-Pawlis, *J. Biol. Inorg. Chem.* **2021**, *26*, 249; c) G. J. Karahalios, A. Thangavel, B. Chica, J. Bacsa, R. B. Dyer, C. C. Scarborough, *Inorg. Chem.* **2016**, *55*, 1102.

- [15] P. Haack, C. Limberg, K. Ray, B. Braun, U. Kuhlmann, P. Hildebrandt, C. Herwig, *Inorg. Chem.* **2011**, *50*, 2133.
- [16] J. Manzur, A. M. García, R. Letelier, E. Spodine, O. Peña, D. Grandjean, M. M. Olmstead, B. C. Noll, *J. Chem. Soc., Dalton Trans.* **1993**, *74*, 905.
- [17] A. M. Barrios, S. J. Lippard, *J. Am. Chem. Soc.* **1999**, *121*, 11751.
- [18] Q.-F. Chen, K.-L. Xian, H.-T. Zhang, X.-J. Su, R.-Z. Liao, M.-T. Zhang, *Angew. Chem. Int. Ed.* **2024**, *63*, e202317514.
- [19] A. Koch, T. A. Engesser, F. Tuczek, *Organometallics* **2023**, *42*, 1774.
- [20] J. R. Cubanski, S. A. Cameron, J. D. Crowley, A. G. Blackman, *Dalton Trans.* **2013**, *42*, 2174.
- [21] V. Gierz, C. Maichle-Mössmer, D. Kunz, *Organometallics* **2012**, *31*, 739.
- [22] Crystallographic data for the structures reported in this article have been deposited at the Cambridge Crystallographic Data Centre under the deposition number CCDC-2149824 and CCDC-2419891 and can be obtained free of charge via http://www.ccdc.cam.ac.uk/data_request/cif.
- [23] F. Weigend, R. Ahlrichs, *Phys. Chem. Chem. Phys.* **2005**, *7*, 3297.
- [24] J. P. Perdew, K. Burke, M. Ernzerhof, *Phys. Rev. Lett.* **1996**, *77*, 3865.
- [25] J. Kuzelka, S. Mukhopadhyay, B. Spingler, S. J. Lippard, *Inorg. Chem.* **2004**, *43*, 1751.
- [26] I. A. Koval, K. van der Schilden, A. M. Schuitema, P. Gamez, C. Belle, J.-L. Pierre, M. Lüken, B. Krebs, O. Roubeau, J. Reedijk, *Inorg. Chem.* **2005**, *44*, 4372.
- [27] N. N. Murthy, M. Mahroof-Tahir, K. D. Karlin, *Inorg. Chem.* **2001**, *40*, 628.
- [28] L. S. Kau, D. J. Spira-Solomon, J. E. Penner-Hahn, K. O. Hodgson, E. I. Solomon, *J. Am. Chem. Soc.* **1987**, *109*, 6433.
- [29] B. L. Geoghegan, Y. Liu, S. Peredkov, S. Dechert, F. Meyer, S. DeBeer, G. E. Cutsail, *J. Am. Chem. Soc.* **2022**, *144*, 2520.
- [30] N. C. Tomson, K. D. Williams, X. Dai, S. Sproules, S. DeBeer, T. H. Warren, K. Wieghardt, *Chem. Sci.* **2015**, *6*, 2474.
- [31] a) R. C. Walroth, J. T. Lukens, S. N. MacMillan, K. D. Finkelstein, K. M. Lancaster, *J. Am. Chem. Soc.* **2016**, *138*, 1922; b) R. K. Hocking, E. I. Solomon, (Eds.) *Ligand Field and Molecular Orbital Theories of Transition Metal X-ray Absorption Edge Transitions*. In: D. Mingos, P. Day, J. Dahl, Eds. *Molecular Electronic Structures of Transition Metal Complexes I. Structure and Bonding*, Vol. 142. Springer, Berlin, Heidelberg, **2011**.
- [32] J. L. DuBois, P. Mukherjee, T. D. P. Stack, B. Hedman, E. I. Solomon, K. O. Hodgson, *J. Am. Chem. Soc.* **2000**, *122*, 5775.
- [33] J. L. DuBois, P. Mukherjee, A. M. Collier, J. M. Mayer, E. I. Solomon, B. Hedman, T. D. P. Stack, K. O. Hodgson, *J. Am. Chem. Soc.* **1997**, *119*, 8578.
- [34] E. I. Solomon, D. E. Heppner, E. M. Johnston, J. W. Ginsbach, J. Cirera, M. Qayyum, M. T. Kieber-Emmons, C. H. Kjaergaard, R. G. Hadt, L. Tian, *Chem. Rev.* **2014**, *114*, 3659.
- [35] H. V. Obias, Y. Lin, N. N. Murthy, E. Pidcock, E. I. Solomon, M. Ralle, N. J. Blackburn, Y.-M. Neuhold, A. D. Zuberbühler, K. D. Karlin, *J. Am. Chem. Soc.* **1998**, *120*, 12960.
- [36] K. D. Karlin, P. Ghosh, R. W. Cruse, A. Farooq, Y. Gultneh, R. R. Jacobson, N. J. Blackburn, R. W. Strange, J. Zubieta, *J. Am. Chem. Soc.* **1988**, *110*, 6769.
- [37] W. B. Tolman, *Acc. Chem. Res.* **1997**, *30*, 227.
- [38] N. Kindermann, S. Dechert, S. Demeshko, F. Meyer, *J. Am. Chem. Soc.* **2015**, *137*, 8002.
- [39] D. E. Root, M. Mahroof-Tahir, K. D. Karlin, E. I. Solomon, *Inorg. Chem.* **1998**, *37*, 4838.
- [40] G. Battaini, E. Monzani, A. Perotti, C. Para, L. Casella, L. Santagostini, M. Gullotti, R. Dillinger, C. Näther, F. Tuczek, *J. Am. Chem. Soc.* **2003**, *125*, 4185.
- [41] M. Mahroof-Tahir, N. N. Murthy, K. D. Karlin, N. J. Blackburn, S. N. Shaikh, J. Zubieta, *Inorg. Chem.* **1992**, *31*, 3001.
- [42] K. Itoh, H. Hayashi, H. Furutachi, T. Matsumoto, S. Nagatomo, T. Tosha, S. Terada, S. Fujinami, M. Suzuki, T. Kitagawa, *J. Am. Chem. Soc.* **2005**, *127*, 5212.
- [43] S. Teramae, T. Osako, S. Nagatomo, T. Kitagawa, S. Fukuzumi, S. Itoh, *J. Inorg. Biochem.* **2004**, *98*, 746.
- [44] L. Li, A. A. Narducci Sarjeant, M. A. Vance, L. N. Zakharov, A. L. Rheingold, E. I. Solomon, K. D. Karlin, *J. Am. Chem. Soc.* **2005**, *127*, 15360.
- [45] L. Li, A. A. N. Sarjeant, K. D. Karlin, *Inorg. Chem.* **2006**, *45*, 7160.
- [46] K. D. Karlin, Y. Gultneh, J. C. Hayes, J. Zubieta, *Inorg. Chem.* **1984**, *23*, 519.
- [47] H.-G. Korth, P. Mulder, *J. Org. Chem.* **2013**, *78*, 7674.
- [48] a) W. B. Tolman, *Angew. Chem. Int. Ed.* **2010**, *49*, 1018; b) M.-L. Tsai, R. G. Hadt, P. Vanelderen, B. F. Sels, R. A. Schoonheydt, E. I. Solomon, *J. Am. Chem. Soc.* **2014**, *136*, 3522; c) S. R. Pauleta, M. S. Carepo, I. Moura, *Coord. Chem. Rev.* **2019**, *387*, 436.
- [49] N. Kitajima, T. Koda, Y. Moro-oka, *Chem. Lett.* **1988**, *17*, 347.
- [50] a) M. R. Churchill, G. Davies, M. A. El-Sayed, J. A. Fournier, J. P. Hutchinson, J. A. Zubieta, *Inorg. Chem.* **1984**, *23*, 783; b) G. Davies, M. A. El-Sayed, M. Henary, *Inorg. Chem.* **1987**, *26*, 3266; c) M. A. El-Sayed, A. El-Toukhy, G. Davies, *Inorg. Chem.* **1985**, *24*, 3387.
- [51] a) N. D. Yordanov, D. Shopov, *J. Inorg. Nucl. Chem.* **1976**, *38*, 137; b) S. Torelli, C. Belle, I. Gautier-Luneau, J. L. Pierre, E. Saint-Aman, J. M. Latour, L. Le Pape, D. Luneau, *Inorg. Chem.* **2000**, *39*, 3526; c) R. Pogni, M. C. Baratto, E. Busi, R. Basosi, *J. Inorg. Biochem.* **1999**, *73*, 157; d) J. Klingele, B. Moubaraki, K. S. Murray, J. F. Boas, S. Brooker, *Eur. J. Inorg. Chem.* **2005**, *1530*; e) A. Kumar Singh, J. I. van der Vlugt, S. Demeshko, S. Dechert, F. Meyer, *Eur. J. Inorg. Chem.* **2009**, 3431.
- [52] a) W. Adam, Y. Y. Chan, D. Cremer, J. Gauss, D. Scheutzow, M. Schindler, *J. Org. Chem.* **1987**, *52*, 2800; b) W. Adam, J. Bialas, L. Hadjarapoglou, *Chem. Ber.* **1991**, *124*, 2377; c) *Org. Synth.* **2013**, *90*, 350; d) E. Poverenov, I. Efremenko, A. I. Frenkel, Y. Ben-David, L. J. W. Shimon, G. Leitun, L. Konstantinovski, J. M. L. Martin, D. Milstein, *Nature* **2008**, *455*, 1093.
- [53] G. Ali, P. E. VanNatta, D. A. Ramirez, K. M. Light, M. T. Kieber-Emmons, *J. Am. Chem. Soc.* **2017**, *139*, 18448.
- [54] X. Zhang, F. G. Bordwell, *J. Org. Chem.* **1992**, *57*, 4163.
- [55] M. A. Ehudin, D. A. Quist, K. D. Karlin, *J. Am. Chem. Soc.* **2019**, *141*, 12558.
- [56] H.-G. Korth, P. Mulder, *J. Org. Chem.* **2020**, *85*, 2560.
- [57] F. G. Bordwell, J. Cheng, G. Z. Ji, A. V. Satish, X. Zhang, *J. Am. Chem. Soc.* **1991**, 9790.

Manuscript received: May 9, 2025

Version of record online: June 3, 2025